

A Monte Carlo calculation model of electronic portal imaging device for transit dosimetry through heterogeneous media

Jihyung Yoon, Jae Won Jung, Jong Oh Kim, and Inhwan Yeo

Citation: *Medical Physics* **43**, 2242 (2016); doi: 10.1118/1.4945276

View online: <http://dx.doi.org/10.1118/1.4945276>

View Table of Contents: <http://scitation.aip.org/content/aapm/journal/medphys/43/5?ver=pdfcov>

Published by the [American Association of Physicists in Medicine](#)

Articles you may be interested in

[Fast transit portal dosimetry using density-scaled layer modeling of aSi-based electronic portal imaging device and Monte Carlo method](#)

Med. Phys. **39**, 7593 (2012); 10.1118/1.4764563

[Monte Carlo calculations of correction factors for plastic phantoms in clinical photon and electron beam dosimetry](#)

Med. Phys. **36**, 2992 (2009); 10.1118/1.3151809

[A Monte Carlo based three-dimensional dose reconstruction method derived from portal dose images](#)

Med. Phys. **33**, 2426 (2006); 10.1118/1.2207315

[Monte Carlo portal dosimetry](#)

Med. Phys. **32**, 3228 (2005); 10.1118/1.2040709

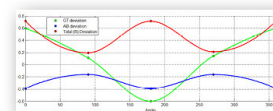
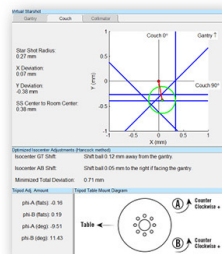
[Verification of treatment parameter transfer by means of electronic portal dosimetry](#)

Med. Phys. **31**, 341 (2004); 10.1118/1.1640972

**Achieve
Sub Millimeter
Accuracy**



- Fast and accurate EPID-based measurement of isocenter position
- Characterization of gantry, couch, and collimator rotation
- Calculates optimization of couch axis automatically
- Compatible with MLC, jaw, or cone based fields of all sizes



New - Eliminate your need for films, and increase your accuracy by using the all new Virtual Starshot, reconstructed using a set of Winston-Lutz images! US Patent 9,192,784

A Monte Carlo calculation model of electronic portal imaging device for transit dosimetry through heterogeneous media

Jihyung Yoon and Jae Won Jung^{a)}

Department of Physics, East Carolina University, Greenville, North Carolina 27858

Jong Oh Kim

Department of Radiation Oncology, University of Pittsburgh Cancer Institute, Pittsburgh, Pennsylvania 15232

Inhwan Yeo

Department of Radiation Medicine, Loma Linda University Medical Center, Loma Linda, California 92354

(Received 21 December 2015; revised 21 February 2016; accepted for publication 21 March 2016; published 6 April 2016)

Purpose: To develop and evaluate a fast Monte Carlo (MC) dose calculation model of electronic portal imaging device (EPID) based on its effective atomic number modeling in the XVMC code.

Methods: A previously developed EPID model, based on the XVMC code by density scaling of EPID structures, was modified by additionally considering effective atomic number (Z_{eff}) of each structure and adopting a phase space file from the EGSnrc code. The model was tested under various homogeneous and heterogeneous phantoms and field sizes by comparing the calculations in the model with measurements in EPID. In order to better evaluate the model, the performance of the XVMC code was separately tested by comparing calculated dose to water with ion chamber (IC) array measurement in the plane of EPID.

Results: In the EPID plane, calculated dose to water by the code showed agreement with IC measurements within 1.8%. The difference was averaged across the in-field regions of the acquired profiles for all field sizes and phantoms. The maximum point difference was 2.8%, affected by proximity of the maximum points to penumbra and MC noise. The EPID model showed agreement with measured EPID images within 1.3%. The maximum point difference was 1.9%. The difference dropped from the higher value of the code by employing the calibration that is dependent on field sizes and thicknesses for the conversion of calculated images to measured images. Thanks to the Z_{eff} correction, the EPID model showed a linear trend of the calibration factors unlike those of the density-only-scaled model. The phase space file from the EGSnrc code sharpened penumbra profiles significantly, improving agreement of calculated profiles with measured profiles.

Conclusions: Demonstrating high accuracy, the EPID model with the associated calibration system may be used for *in vivo* dosimetry of radiation therapy. Through this study, a MC model of EPID has been developed, and their performance has been rigorously investigated for transit dosimetry.

© 2016 American Association of Physicists in Medicine. [<http://dx.doi.org/10.1118/1.4945276>]

Key words: transit dosimetry, Monte Carlo, EPID, heterogeneous media, XVMC

1. INTRODUCTION

Offering on-line transit dose, electronic portal imaging devices (EPIDs) have been employed for *in vivo* dosimetry of radiation deliveries.^{1–4} For treatment verification using EPID, various computational models of the dose image of EPID have been developed.^{5–18} Among them, the most utilized models are characterized by the use of kernels that are predetermined dose responses of primary and scattered fluences in EPID.^{5–12} The kernel-based models have been widely used because of their fast calculation speed and reasonable accuracy. The accuracy of the models was improved by employing kernels based on Monte Carlo (MC) simulations of EPID.^{13–15}

A continuous effort was exerted to achieve the maximum possible accuracy by modeling details of actual structures of EPID and their elemental compositions in a Monte Carlo code. The model allowed direct radiation transport through the

structures without utilizing the kernels. Among them, Siebers *et al.* modeled EPID (aS500 Varian Medical Systems, Inc.) with a virtual detector¹⁶ technique utilizing detector grids in the dose calculation region only, instead of performing voxelized calculations across the entire radiation transport media, inherent in the EGS4/DOSXYZ user code,¹⁹ that require a longer calculation time. The model was not tested under phantoms of clinical relevance. The test, however, is necessary for its application in transit dose verification (i.e., transit dosimetry). This is because the transit dose calculation demands a higher degree of accuracy from calculation algorithms than EPID calculation, without intervening phantoms, does by involving radiation transport through heterogeneous media and air gaps to the plane of EPID. Such model, therefore, in principle could be vulnerable to changes in phantom and air gap thicknesses and the related scattering contributions.^{20,21}

A simplified and fast calculation model of EPID based on MC transport for transit dosimetry was introduced by Jung *et al.*²² The model incorporates structural and elemental compositions of EPID (aS1000) by homogenized (i.e., water) layers in the XVMC code.²³ To account for heterogeneity in the actual composition of EPID structures, each homogeneous layer was assigned the physical density of the corresponding structure. While the model produced acceptable accuracy in a relatively fast computation time, it generated EPID image responses that are highly dependent on the variation of attenuation thicknesses in patient, thus requiring thickness-dependent factors that account for differences between measured and calculated EPID images. The model also showed limited agreement in the region of beam penumbra.

In this study, for transit dosimetry applications, we have improved the EPID model²² in the XVMC code by considering the effective atomic number of each EPID layer and more accurate beam spectra. We have performed twofold evaluation of the model by investigating the accuracy of the MC code in water and that of the model in the transit dose plane under homogeneous and heterogeneous media. The twofold evaluation was intended to distinguish the sources of error in the plane of the EPID between the MC code and the EPID model, offering better understanding of the performance of the model. The evaluation of the MC code and the MC model of EPID in the plane of the EPID under intervening phantoms of various thicknesses and heterogeneities was not rigorously investigated before and is necessary for the *in vivo* application of the MC model.²⁴

2. MATERIALS AND METHODS

2.A. Development of the Monte Carlo model of EPID

The realistic structures of EPID (Ref. 16) could not be reproduced in the XVMC code, which defines structures by finite-sized voxels composed of water-equivalent materials.²³ Therefore, the thickness and elemental composition of each layer of EPID were alternatively modeled in the XVMC code. This was partly achieved by density scaling described in Eq. (1) in our previous study,²²

$$\rho_{\text{scaled}} = \frac{1}{t} \sum_i (\rho_i \times t_i), \quad (1)$$

where ρ_{scaled} and t are the scaled physical density and thickness of a layer in the model, respectively; ρ_i and t_i are the actual physical density and the thickness of an i th physical layer of EPID, respectively. In the model, if the thicknesses of the layers were smaller than the dimension of the voxel, multiple layers as indicated by the index “ i ” comprised a single-voxel layer. In the current study, in addition to the previous scaling method, the elemental compositions of the structures were also considered to improve the model.

A probability of Compton interaction in a medium is proportional to its number of electrons per unit volume (e/cm^3), which can be expressed by multiplication of the

physical density (mass per unit volume) and the electron density (number of electrons per unit mass).^{25,26} The electron density per unit mass is proportional to Z/A , where Z and A are the atomic and the mass numbers of the medium, respectively. Since the electron densities per unit mass of lung, soft tissue, and bone are similar (the cortical bone is thin as well), the physical density-only scaling is acceptable for them. To model high- Z materials in the XVMC code, however, the value of Z/A relative to that of water should be considered in the scaling process. For each layer of EPID, the effective atomic number Z_{eff} was computed, and then a normalized Z_{eff}/A value to that of water, noted as $Z_{\text{eff}}^n(E)$, was determined by the Auto- Z_{eff} software,²⁷ considering the physics of Compton scattering in the layer for a given photon energy E . The average photon energy at 150 cm was determined from the exit fluence calculations performed by the EGSnrc/BEAMnrc code.²⁸ In order to perform calculation, the input photon source terms were prepared by generating 6 MV phase space data for various field sizes under the Varian Linac head from the code. The generated phase space data were then used to calculate the exit fluence under various phantoms (phantom-phase space data) and field sizes employed in this study. The average energy ranged between 1.7 and 1.8 MeV for photon beams of varying field sizes of 5×5 to 15×15 cm² that passed through phantoms of thicknesses of 10–30 cm. Therefore, for all conditions, the calculated $Z_{\text{eff},i}^n(E = 1.75 \text{ MeV})$ of each (i th) layer was then multiplied to the density ρ_i to determine the scaled effective density, $\rho_{\text{eff},i}$, in Eq. (2),

$$\rho_{\text{eff},i} = \rho_i \times Z_{\text{eff},i}^n(E = 1.75 \text{ MeV}). \quad (2)$$

By using $\rho_{\text{eff},i}$, the Compton interactions in each layer were more accurately modeled.

Applying the scaled effective density in Eq. (1), we have derived a corrected effective density of a layer in the EPID model in Eq. (3),

$$\rho_{\text{scaled},Z_{\text{eff}}} = \frac{1}{t} \sum_i (\rho_{\text{eff},i} \times t_i), \quad (3)$$

and used it throughout this study. The performance of the corrected model was compared with that of the density-only-scaled model developed previously.²²

In our prior studies, we found that the dose gradient in penumbra areas of simulated EPID images is smaller than that from measurements; the dose gradient across a heterogeneous interface was also smaller than that from measurements as well.^{22,29} Since the XVMC code uses a virtual source model based on the Gaussian spatial distribution in order to reduce calculation time, it may not be physically accurate near field edges.³⁰ To improve the performance in the penumbra, we have employed the above phase space data generated from the EGSnrc code. The phase space data were irradiated to calculate two-dimensional (2D) EPID dose images in the phosphor layer of the XVMC model. The calculations were done for each phantom and field size employed in this study. The calculations with the XVMC code involved only a one-step process of full 3D voxelized dose calculation from the phase space above phantoms to the EPID model.

2.B. Validation of the EPID models

The source of errors between calculations and measurements could be attributed to the exit fluence accuracy in the plane of EPID that is governed by the fundamental physics model of the radiation transport through phantom and air gap layers of various thicknesses. In addition, it could be affected by potentially imprecise and/or inaccurate simulation of the actual structural and elemental compositions of the EPID under study. Therefore, we have separated the validation of the EPID model into two steps: (1) validation of the code with measured absolute doses to water in the plane of EPID under homogeneous and heterogeneous phantoms and (2) the validation of the EPID model with EPID measurements. The result of the second step contains the two sources of errors described above.

2.B.1. Dose to water in the plane of EPID: Monte Carlo code validation

Doses were measured in an ion chamber (IC) array (OCTAVIUS 729, PTW, Freiburg, Germany) that was placed under a 2-cm thick buildup layer, including the inherent buildup, and above a 5-cm thick backup phantom. The source-to-detector plane distance (SDD) was 150 cm. Photon beams with an energy of 6 MV (2100iX, Varian Medical Systems, Palo Alto, CA), a dose of 200 MUs, a dose rate of 300 MU/min, and field sizes of 5×5 , 10×10 , and 15×15 cm² were irradiated through various phantoms to the array as shown in Fig. 1. Since the IC array has a 1-cm resolution with the individual IC dimension of $0.5 \times 0.5 \times 0.5$ cm³, we repeated measurements after shifting the IC array diagonally by a half of the IC interspacing and merged the two measurements, doubling the

TABLE I. Thickness configurations of the heterogeneous phantoms.

	Lung		Bone	
Total thickness (cm)	15	25	13	23
Upper water phantom	5.0	10.0	5.0	10.0
Lung/bone phantom	5.0	5.0	3.0	3.0
Lower water phantom	5.0	10.0	5.0	10.0

resolution. The IC array was precalibrated to absolute dose at the isocenter and at the depth of 10 cm.

The phantoms included homogeneous and heterogeneous phantoms that were isocentrically placed as shown in Figs. 1(a) and 1(b), respectively. The former was homogeneous plastic water phantoms (CIRS, Inc., Norfolk, VA) of various thicknesses (10, 20, and 30 cm). The latter was constituted of a 3-cm thick bone phantom or a 5-cm thick lung phantom (Gammex, Inc., Middleton, WI) that was placed with its edges aligned to the beam axis while being sandwiched between homogeneous plastic water phantoms. Detailed phantom thicknesses for the heterogeneous phantoms are listed in Table I.

Monte Carlo simulations were performed using the same conditions as the above setups. The phantoms of plastic water, lung, and bone used in the experiments were CT scanned and imported into the XVMC code for the simulations. The IC array with buildup and backup phantoms was replaced with a 7-cm thick water phantom in the simulation, and doses were calculated at a 2-cm depth. For comparison, the calculation voxel size was kept the same as the IC size ($0.5 \times 0.5 \times 0.5$ cm³). The calculated doses by the code had been precalibrated to the absolute dose at the isocenter and at the depth of the dose maximum. The statistical uncertainty of all calculations in this

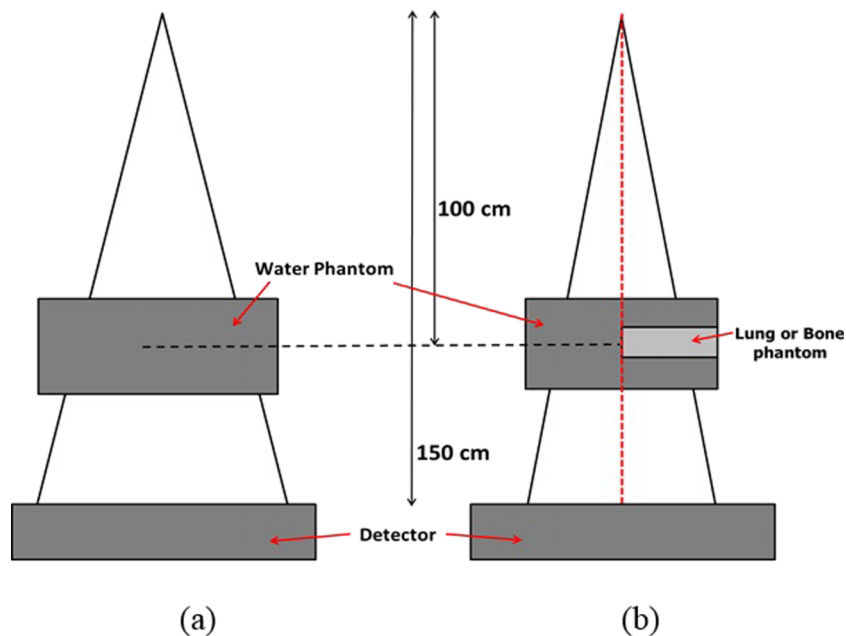


FIG. 1. Experimental setups with (a) the homogeneous phantoms and (b) the heterogeneous phantoms. The phantoms were isocentrically placed, and the detectors (IC array or EPID) were placed at 150 cm. Phantom thicknesses were 10, 20, and 30 cm for the homogeneous phantom. The thicknesses of the lung and the bone phantoms were 5 and 3 cm, respectively. They were sandwiched by water phantoms of thicknesses 5 and 10 cm.

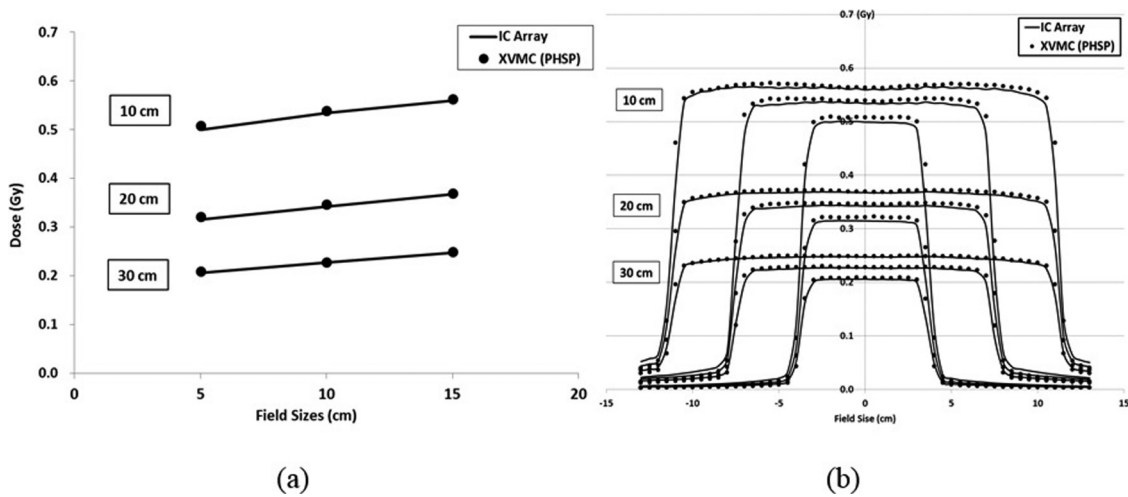


FIG. 2. Intercomparison of absolute dose to water by the XVMC calculations and IC array measurements in the EPID plane under homogeneous phantoms. (a) Doses at the beam axis. (b) Off-axis dose profiles. Phantom thicknesses of 10, 20, and 30 cm and field sizes of 5×5, 10×10, and 15×15 cm² were used. Each graph displays results measured by ion chamber array and results calculated by the code (with the phase space source model).

study was kept within 0.5% at the beam axis. The calculation results were compared with the measurements.

The patient couch was not modeled in the simulation; instead, a measured couch attenuation factor was determined and applied to the simulation results.

2.B.2. Dose to EPID: EPID model validation

Measurements of EPID dose images were performed for the same experimental conditions used in the dose-to-water measurements as shown in Fig. 1. Prior to measurements, the EPID was calibrated by background noise cancellation and gain correction. The 2D pixel-to-pixel correlation between the calculated EPID dose images and the measured images at 150 cm from the target was performed under a 20-cm thick phantom and the field size of 27.2×20.8 cm², generating a 2D calibration matrix. The calibration matrix was then scaled to represent each condition of measurement, i.e., the field size of irradiation and phantom thickness, to provide a condition-dependent pixel-to-pixel calibration matrix. For the measurements, the integration mode of image acquisition, the dose of 200 MUs, and the dose rate of 300 MU/min were used. Details of the calibration and measurement procedures are provided in our prior study.²²

For each of the experimental conditions, the EPID image was also calculated on the MC model of EPID for comparative evaluations. The calculated images were then converted to measured images using the calibration matrix obtained and scaled above. In the EPID calculations, the patient couch was not modeled, because the couch was not modeled when the calibration matrix was generated. Therefore, neglecting the patient couch did not affect the final value of the converted images from the calculations. In addition, the supporting arm behind the EPID was not modeled, because it was not modeled when the calibration matrix was generated, thereby incorporating the effect of the backscattering from the arm in the converted images from the calculations. The pixel size of the calculations was 0.25×0.25 cm²; the raw pixel size of

EPID images was rescaled to it for comparison. For the EPID model, the thickness of the phosphor layer was 0.25 cm.

3. RESULTS AND DISCUSSION

3.A. Dose to water in the plane of EPID: Monte Carlo code validation

3.A.1. Under homogeneous phantoms

Absolute doses to water at the beam axis measured by the IC array and those calculated by the MC simulations were intercompared for various phantom thicknesses and field sizes, as shown in Fig. 2(a) and Table II. The couch attenuation was determined to be 2.3%, averaged over field sizes of 5×5 to 15×15 cm² and phantom thicknesses of 0–30 cm, and was applied to all dose-to-water calculations in this study.

Table II showed that the maximum difference of the XVMC code was +1.6% for the field size of 15×15 cm² under the 10-cm thick phantom. At the depths of 10, 20, and 30 cm in water (isocentrically setup) and under the field size of 10×10 cm², the XVMC code responded to IC measurements with the differences of +0.3%, -0.1%, and -0.3%, respectively (i.e., commissioning accuracy of the code). From the above differences, we found that in the plane of EPID, placed at 150 cm via air gap, the code provided increased differences, as shown in Table II, by producing greater relative responses to the ion chamber responses for each thickness, for example, the difference of +1.4% vs

TABLE II. Differences between calculated doses by the XVMC code and measured doses in the IC array of irradiations through homogeneous phantoms at the beam axis in the EPID plane.

Field size (cm ²)	10 cm	20 cm	30 cm
5 × 5	0.8%	1.3%	0.4%
10 × 10	1.0%	1.4%	0.5%
15 × 15	1.6%	1.3%	1.3%

TABLE III. Summary of maximum average and maximum point differences across in-field regions in the plane of EPID between calculated doses by the XVMC code and measured doses in the IC array and EPID, respectively, of irradiations through homogeneous and heterogeneous phantoms.

Detector	Medium		Difference (%)	Field size (cm ²)	Phantom thickness (cm)	Location
IC array	Homogeneous	Maximum average	1.8	15 × 15	20	—
		Maximum point	2.8	15 × 15	20	—
	Heterogeneous	Maximum average	1.7	15 × 15	13 (bone)	Bone
		Maximum point	2.7	15 × 15	13 (bone)	Bone
EPID	Homogeneous	Maximum average	0.4	5 × 5	30	—
		Maximum point	1.2	5 × 5	30	—
	Heterogeneous	Maximum average	1.3	5 × 5	15 (lung)	Lung
		Maximum point	1.9	5 × 5	15 (lung)	Lung

−0.1% for the code at the condition of a 20-cm thickness and 10 × 10 cm². In spite of the above variations, overall, the results of MC calculations showed small errors, less than the above maximum 1.6%. We believe that the differences, found above and throughout this study, have been contributed by the level of the fundamental accuracy achievable by the code (stated in Sec. 2.B), affected by the commissioning accuracy.

Off-axis profiles were intercompared between calculations and measurements in Fig. 2(b). All profiles presented in this study were obtained from the cross-plane direction; evaluations of in-plane profiles were not much different. The average difference was acquired as an average of differences at all data points across the in-field region (excluding penumbra area; 1 cm away from the half maximum), with a maximum standard deviation of 0.5%, for each profile throughout this study. Among the average differences for all conditions and profiles, the maximum average differences were found to be 1.8% for the code under the thickness of 20 cm as shown in Table III. The maximum point differences were found to be 2.8% under the same condition.

Calculated dose-to-water profiles by the code based on the virtual source and the phase space models were compared with IC array measurements in the EPID plane in Fig. 3. The

phase space model provided a slightly better agreement in the in-field region and sharpened penumbra profiles. We need to note that the XVMC code with its inherent virtual source model is optimized for dose calculation in a water medium, and thus the virtual source model still provides a good agreement with measurements in water.³⁰

3.A.2. Under heterogeneous phantoms

Absolute dose profiles under the heterogeneous phantoms are shown in Fig. 4. The profiles are quantitatively evaluated in Table IV in terms of average differences between the calculations and the measurements. The average differences were sampled across the in-field region (excluding penumbra and interface between water and lung/bone phantoms; 1 cm away from the center of each dose gradient region). As shown in Table III, the XVMC code yielded a maximum average difference of 1.7% and a maximum point difference of 2.7% in the bone-phantom side when the field size of 15 × 15 cm² and the total phantom thickness of 13 cm were used.

As shown in Table IV, we found that the average differences of the XVMC calculations are different between the lung and the water sides for all field sizes and thicknesses (the differences are noteworthy). This came from the fact that the relative outputs of the calculations to the IC outputs were smaller in the lung side than those under the water side. This finding could be contributed by the limited accuracy reported for XVMC calculations in lung materials.²³ Overall, the XVMC results showed good agreement with the IC array measurements within the above maximum error of 2.8% (stated in Sec. 3.A.1 and Table III).

3.B. Dose to EPID: EPID model validation

3.B.1. Under homogeneous phantoms

Figure 5 shows ratios of measured pixel values of EPID to calculated doses in the EPID model at the central axis. The former is proportional to the dose deposited in the phosphor layer that is placed in front of the image sensor.¹⁶ Therefore, the ratios conceptually imply response characteristics of EPID measurements relative to its simulations. The ratios in this study functioned as scale factors for dose-to-pixel

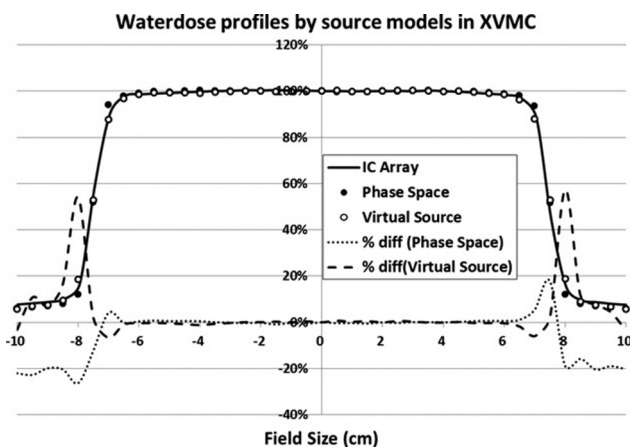


FIG. 3. Intercomparison of calculated dose-to-water profiles with a phase space model and those with a virtual source model with reference to measurement by the IC array. The experimental condition was under a 20-cm thickness homogeneous phantom and the field size of 10 × 10 cm². The penumbra slope was slightly steeper when the phase space file was used.

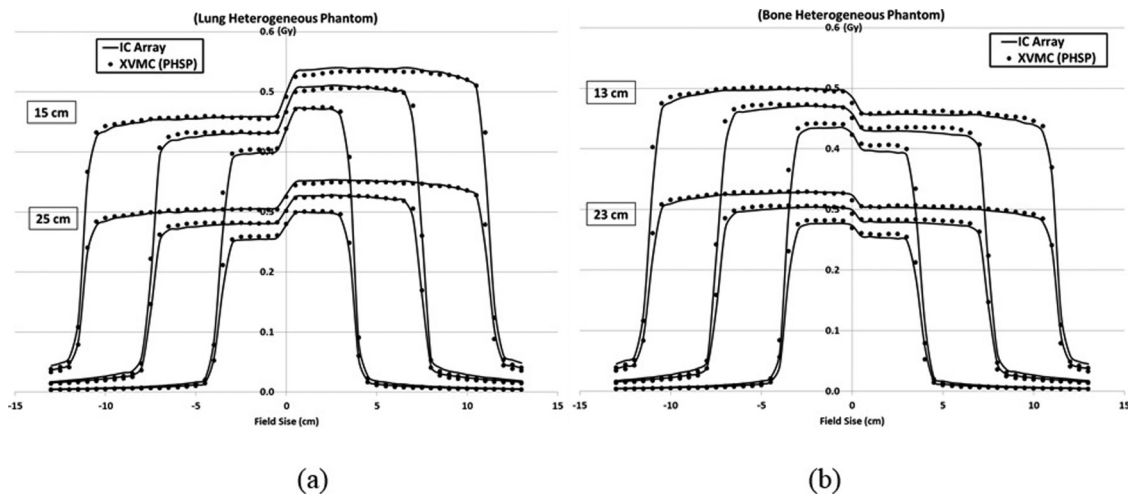


FIG. 4. Intercomparison of absolute dose-to-water profiles of MC calculations and IC array measurements across the EPID plane under (a) heterogeneous lung and (b) bone phantoms for field sizes of 5×5 , 10×10 , and 15×15 cm². Profiles for two sets of phantom thicknesses were provided in each graph. Each graph displays the profile measured by the IC array and that calculated by the XVMC code. In each graph, the left half was under the water-equivalent phantoms and the right half was under the lung or bone sandwiched slabs.

value conversions that are dependent on field sizes and phantom thicknesses. In the figure, they were normalized at the condition of the field size of 10×10 cm² and the thickness of 20 cm at which 2D dose-to-image calibration was performed. Across all thicknesses and field sizes, the factors varied between 0.93 and 1.06 for the EPID model. The model showed that the calculated dose/the measured pixel values (reciprocal of the factor) decreased as the field size increased. This is similar to the trend of calculated dose/measured dose in water that can be obtained from the trends in Table II and Fig. 2(a). However, the dependence of the factors on field-size changes was much greater in the EPID model. In spite of the more realistic modeling of EPID, the variance of the factors may imply deficiency in the accuracies of EPID modeling. That is, explicit modeling of elemental composition could not be done.

Profiles of calculated dose images and measured images in EPID for various phantom thicknesses and field sizes were shown in Fig. 6. The maximum average difference of the EPID model was 0.4%, and the maximum point difference was 1.2% within the in-field regions as shown in Table III. They were

TABLE IV. Differences between calculated and measured doses (IC array) to water in the EPID plane under heterogeneous phantoms. In-field average differences in the regions under the water phantoms and the lung or bone phantoms (non-water) were shown.

Field size	Phantom side	Lung (%)		Bone (%)	
		15 cm	25 cm	13 cm	23 cm
5 × 5	Water	0.5	0.8	0.7	0.9
	Non-water	-0.7	-0.3	1.4	1.0
10 × 10	Water	0.7	0.9	0.8	1.0
	Non-water	-0.5	-0.2	1.5	1.5
15 × 15	Water	1.1	1.2	1.3	1.4
	Non-water	0	0.2	1.7	1.7

found under the 30-cm thick phantom and the field size of 5×5 cm². The penumbra profiles of the model matched well with the measurements. The above small differences came from the calibration based on the above scale factors, unlike the response of the code in the plane of EPID that showed greater differences.

A noticeable change between the previous density-scaled XVMC model²² and the new Z_{eff} -corrected XVMC model is that the factors of the new model showed an increasing trend as field sizes increase, while the factors of the previous model showed a minimum at an intermediate field size. This new trend is encouraging because the calibration factors (Fig. 5) show a trend approaching linearity. This finding was not affected by the choice of the source models. In addition, a significant change (i.e., improvement) in penumbra profile

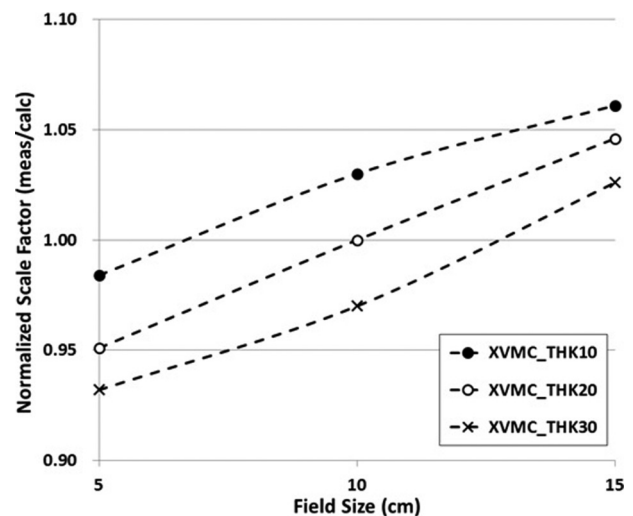


FIG. 5. Scale factors (i.e., ratios) of measured pixel values of EPID to calculated dose in the XVMC model of EPID as functions of field size and phantom thickness. The factors were normalized at the field size of 10×10 cm² under a 20-cm thick phantom at which 2D dose-to-image calibration was performed.

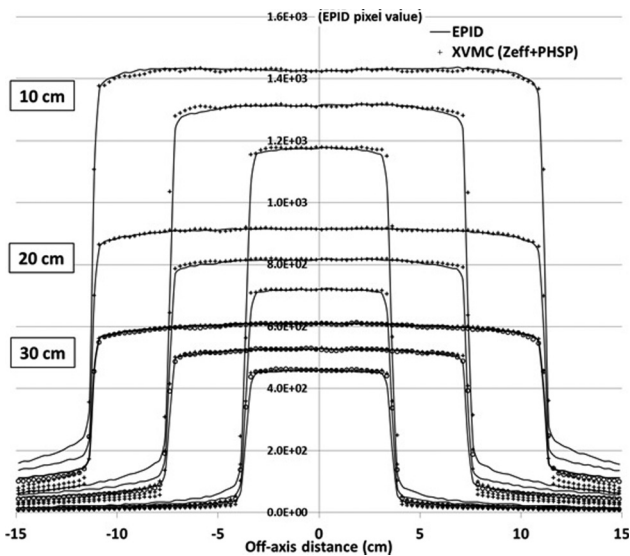


FIG. 6. Intercomparison of EPID image profiles by calculations in the XVMC model of EPID and measurements in EPID under homogeneous phantoms. The phantom thicknesses of 10, 20, and 30 cm were used; the field sizes were 5×5 , 10×10 , and 15×15 cm². The calculations were done with the Z_{eff} structure model and the phase space source model.

calculations was made as shown in Fig. 7 by employing the phase space file from the EGSnc code. This change can be explained by the fact that the inherent virtual source model is optimized for dose calculation in water equivalent or similar materials only³⁰ and thus is not suitable for modeling beam profiles measured in such heterogeneous media of EPID (compare Fig. 7 with Fig. 3).

All calculations in this study were performed by a computer equipped with 6 core 2.93 GHz Intel Xeon CPUs and 12 GB RAM. The total calculation time for the condition of a 20-cm thick homogeneous phantom and the field size of 10×10 cm² was 1.2 h for the XVMC model.

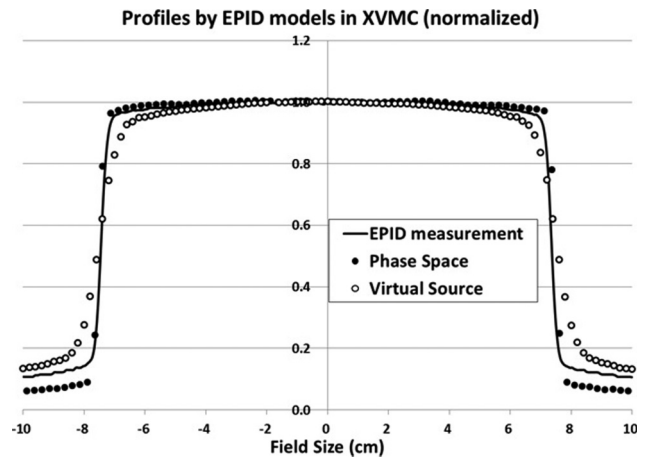


FIG. 7. Intercomparison of EPID image profiles calculated in the XVMC model with the phase space source model, those with the virtual source model and the profiles measured in EPID for the field size of 10×10 cm² and a 20-cm thick homogeneous phantom. The profiles were normalized at the beam axis.

3.B.2. Under heterogeneous phantoms

Calculated EPID dose images were similarly compared with measured images for the heterogeneous phantoms and field sizes employed in this study in Fig. 8 and Table V. The comparison showed the maximum average difference less than 1.3% for the EPID model for all conditions as shown in Table III. The maximum was found under the lung side of the 15-cm thick phantom with the field size of 5×5 cm². The maximum point difference was 1.9% under the same condition.

Similarly to the performance in the water phantom, the EPID model produced different amounts of differences between the lung and the water sides for each field size and thickness: of note, the differences were -1.3% vs $+0.3\%$, -1% vs $+0.5\%$, and -1.1% vs $+0.2\%$ for the field sizes of 5×5 , 10×10 , and 15×15 cm², respectively, for the case of the

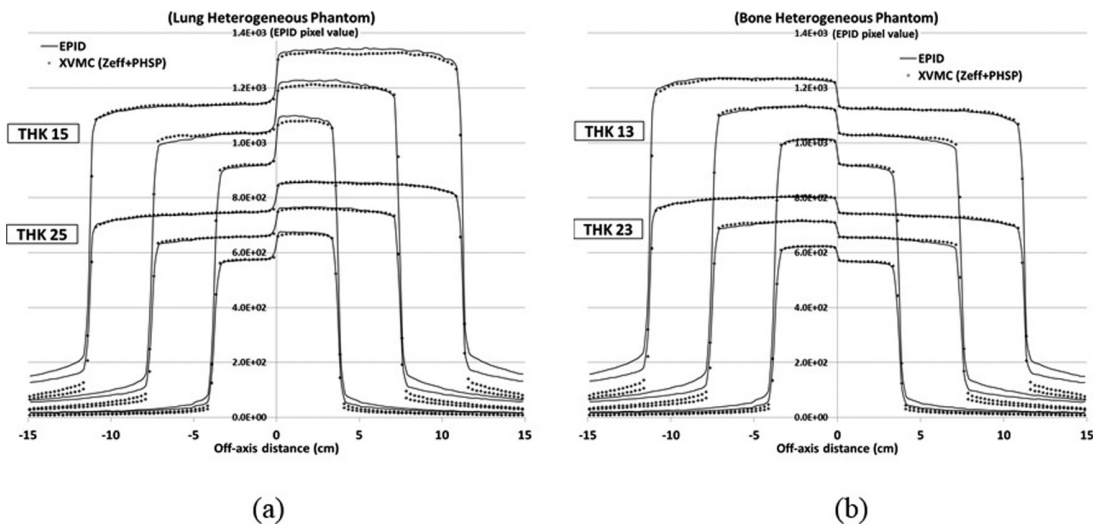


FIG. 8. EPID image profile intercomparison under the calculations of the XVMC model and measurements under (a) heterogeneous lung and (b) bone phantoms for field sizes of 5×5 , 10×10 , and 15×15 cm². Profiles for two sets of phantom thicknesses were provided in each graph. In each graph, the left half was under the water-equivalent phantoms and the right half was under the lung or bone sandwiched slabs. The calculations were done in the EPID model with the Z_{eff} structure model and phase space source model.

TABLE V. Differences between calculated and measured EPID images under heterogeneous phantoms. Average differences were shown between the calculations and measurements in the regions under the water phantom and the lung or bone phantom (non-water).

Field size	Phantom side	Lung (%)		Bone (%)	
		15 cm	25 cm	13 cm	23 cm
5 × 5	Water	0.3	0.0	-0.3	-0.1
	Non-water	-1.3	-0.9	0.3	0.2
10 × 10	Water	0.5	0.1	0.1	0.4
	Non-water	-1.0	-0.5	0.4	0.3
15 × 15	Water	0.2	0.1	-0.3	<0.1
	Non-water	-1.1	-0.2	0.2	<0.1

15-cm thick phantom as shown in Table V. The differences of the EPID model under the lung phantom were greater for the thinner phantom (15 cm thick) than for the thicker phantom (25 cm thick): of note, the differences were -1.3% vs -0.9%, -1.0% vs -0.5%, and -1.1% vs -0.2% for the field sizes of 5×5, 10×10, and 15×15 cm², respectively. The findings above may be explained in the following. The EPID images (i.e., pixel values) were obtained from calculated doses in the model through calibration that is dependent on field sizes and thicknesses of the water phantoms (not the lung/bone side). Therefore, greater differences were expected on the lung/bone side. This, however, did not have much impact on the results in Table V, given the small differences between the effective thicknesses of the lung/bone side and those of the water side tried in this study. In support of this argument, the trend of data (differences under the lung/bone phantoms compared with those under the water phantoms for the two codes) in Table IV appeared to be extended to that in Table V with one exception, the EPID model under the 25-cm lung phantom and the field size of 15×15 cm². Thus, the trend of the above data was contributed mainly by the performance of the code, affected by the fundamental MC accuracy (discussed in Sec. 3.B) and secondarily by the calibration adopted in this study. Note that this argument is applicable to the level of heterogeneity of phantoms tried in this study; in reality, the effective thicknesses in patients could be more variable.

As shown in Table III, the maximum average differences and the maximum point differences were reduced from the calculations in water to the calculations in the EPID model for all conditions of field sizes and thicknesses (compare 2.8% for the XVMC code with 1.9% for the code's EPID model).

The application of the Monte Carlo model for transit dosimetry has not been fully investigated before. Studies without phantoms have been done, but studies with intervening phantoms are not found in major journals to our knowledge. While the XVMC code is relatively accurate within phantoms and in the water phantom at the plane of EPID that is separated from intervening phantoms via air gaps (i.e., transit condition), in the EPID model (although improved) in the transit condition, it was found not to be as accurate by our study. In this regard, the understanding gained by this study including the quantified performance of the code (code itself

and EPID model) in the transit condition is beneficial to transit dosimetry.

While the current study is focused on the fundamental evaluation of the EPID models for transit dosimetry, in reality, we will face more complex situations than the conditions tried in this study. In order to apply the scale factors to such situations, we can employ an average field size of each IMRT beamlet and an average phantom thickness within each beamlet or a thickness along each beam ray. In our prior work,²² we have reported successful results based on the first two approaches. More work can be done in this regard, but it is outside of the scope of this study.

4. CONCLUSION

A new computational model of EPID in the XVMC code was developed by incorporating effective atomic numbers of elemental components of EPID structures and adopting the phase space source from the EGSnrc code into the density-scaled model previously developed.²² The XVMC code was found to perform within the accuracy of 2.8% (in point differences) in water phantom at the plane of EPID. The code's EPID model was found to perform dependently on field size and phantom thicknesses by exhibiting the calibration factor (measurements/calculations) variations of +6%/-7%. Using the factors that are dependent on field sizes and thicknesses for the conversion of calculated images to measured images, the model was found to perform within the accuracies of 1.9%. The Z_{eff} correction incorporated into the EPID model improved the physical trends of the calibration factors, compared with that of the density-only-scaled model.²² The use of phase space data from the EGSnrc/BEAMnrc code significantly improved agreement of calculated profiles with measured profiles in penumbra regions. Demonstrating superior accuracy, the EPID model may be used for accurate *in vivo* dosimetry of radiation therapy. Significant amounts of calculation time can be saved by using the model based on the XVMC code that is built for fast calculations in water-equivalent media. Through this study, an MC model of EPID has been developed and its performance has been rigorously investigated for transit dosimetry.

ACKNOWLEDGMENTS

Dr. Jong Oh Kim would like to express appreciation to Dr. Fippel for allowing him to use the XVMC code. The authors thank Christopher Pelletier for his editorial assistantship.

^{a)}Author to whom correspondence should be addressed. Electronic mail: jungj@ecu.edu

¹B. Mijnheer, S. Beddar, J. Izewska, and C. Reft, "In vivo dosimetry in external beam radiotherapy," *Med. Phys.* **40**(7), 070903 (19pp.) (2013).

²A. Piermattei et al., "In vivo dosimetry by an aSi-based EPID," *Med. Phys.* **33**(11), 4414-4422 (2006).

³L. N. McDermott et al., "3D *in vivo* dose verification of entire hypofractionated IMRT treatments using an EPID and cone-beam CT," *Radiother. Oncol.* **86**(1), 35-42 (2008).

- ⁴W. van Elmpt, S. Nijsten, S. Petit, B. Mijnheer, P. Lambin, and A. Dekker, "3D *in vivo* dosimetry using megavoltage cone-beam CT and EPID dosimetry," *Int. J. Radiat. Oncol., Biol. Phys.* **73**(5), 1580–1587 (2009).
- ⁵T. R. McNutt, T. R. Mackie, P. Reckwerdt, N. Papanikolaou, and B. R. Paliwal, "Calculation of portal dose using the convolution/superposition method," *Med. Phys.* **23**(4), 527–535 (1996).
- ⁶V. N. Hansen, W. Swindell, and P. M. Evans, "Extraction of primary signal from EPIDs using only forward convolution," *Med. Phys.* **24**(9), 1477–1484 (1997).
- ⁷K. L. Pasma, B. J. Heijmen, M. Kroonwijk, and A. G. Visser, "Portal dose image (PDI) prediction for dosimetric treatment verification in radiotherapy. I. An algorithm for open beams," *Med. Phys.* **25**(6), 830–840 (1998).
- ⁸B. M. McCurdy and S. Pistorius, "A two-step algorithm for predicting portal dose images in arbitrary detectors," *Med. Phys.* **27**(9), 2109–2116 (2000).
- ⁹L. Spies and T. Bortfeld, "Analytical scatter kernels for portal imaging at 6 MV," *Med. Phys.* **28**(4), 553–559 (2001).
- ¹⁰C. V. Dahlgren, A. Ahnesjö, A. Montelius, and G. Rikner, "Portal dose image verification: Formalism and application of the collapsed cone superposition method," *Phys. Med. Biol.* **47**(24), 4371–4387 (2002).
- ¹¹W. J. C. van Elmpt, S. M. J. G. Nijsten, B. J. Mijnheer, and A. W. H. Minken, "Experimental verification of a portal dose prediction model," *Med. Phys.* **32**(9), 2805–2818 (2005).
- ¹²W. van Elmpt, L. McDermott, S. Nijsten, M. Wendling, P. Lambin, and B. Mijnheer, "A literature review of electronic portal imaging for radiotherapy dosimetry," *Radiother. Oncol.* **88**(3), 289–309 (2008).
- ¹³B. M. McCurdy, K. Luchka, and S. Pistorius, "Dosimetric investigation and portal dose image prediction using an amorphous silicon electronic portal imaging device," *Med. Phys.* **28**(6), 911–924 (2001).
- ¹⁴B. Warkentin, S. Steciw, S. Rathee, and B. G. Fallone, "Dosimetric IMRT verification with a flat-panel EPID," *Med. Phys.* **30**(12), 3143–3155 (2003).
- ¹⁵K. Chytky and B. M. C. McCurdy, "Investigation of tilted dose kernels for portal dose prediction in a-Si electronic portal imagers," *Med. Phys.* **33**(9), 3333–3339 (2006).
- ¹⁶J. V. Siebers, J. O. Kim, L. Ko, P. J. Keall, and R. Mohan, "Monte Carlo computation of dosimetric amorphous silicon electronic portal images," *Med. Phys.* **31**(7), 2135–2146 (2004).
- ¹⁷L. Parent, J. Seco, P. M. Evans, A. Fielding, and D. R. Dance, "Monte Carlo modelling of a-Si EPID response: The effect of spectral variations with field size and position," *Med. Phys.* **33**(12), 4527–4540 (2006).
- ¹⁸E. Spezi and D. G. Lewis, "Full forward Monte Carlo calculation of portal dose from MLC collimated treatment beams," *Phys. Med. Biol.* **47**(3), 377–390 (2002).
- ¹⁹W. R. Nelson, H. Hirayama, and D. W. O. Rogers, "The EGS4 code system," SLAC-265, Stanford Linear Accelerator Center, 1985.
- ²⁰E. Vanetti De' Palma *et al.*, "Experimental method to obtain scattering contribution in portal dose images," *Phys. Med.* **21**(1), 31–40 (2005).
- ²¹P. Rowshanfarzad, M. Sabet, D. J. O'Connor, and P. B. Greer, "Impact of backscattered radiation from the bunker structure on EPID dosimetry," *J. Appl. Clin. Med. Phys.* **13**(6), 91–100 (2012).
- ²²J. W. Jung, J. O. Kim, I. J. Yeo, Y.-B. Cho, S. M. Kim, and S. Dibiase, "Fast transit portal dosimetry using density-scaled layer modeling of aSi-based electronic portal imaging device and Monte Carlo method," *Med. Phys.* **39**(12), 7593–7602 (2012).
- ²³M. Fippel, "Fast Monte Carlo dose calculation for photon beams based on the VMC electron algorithm," *Med. Phys.* **26**(8), 1466–1475 (1999).
- ²⁴I. J. Yeo, J. W. Jung, B. Y. Yi, and J. O. Kim, "Feasibility study on inverse four-dimensional dose reconstruction using the continuous dose-image of EPID," *Med. Phys.* **40**(5), 051702 (11pp.) (2013).
- ²⁵J. W. Penelope and J. Allisy-Roberts, *Farr's Physics for Medical Imaging*, 2nd ed. (Saunders Ltd., Philadelphia, PA, 2007).
- ²⁶F. M. Khan, *The Physics of Radiation Therapy* (Lippincott Williams & Wilkins, Philadelphia, PA, 2003).
- ²⁷M. L. Taylor, R. L. Smith, F. Dossing, and R. D. Franich, "Robust calculation of effective atomic numbers: The Auto-Z_{eff} software," *Med. Phys.* **39**(4), 1769–1778 (2012).
- ²⁸D. W. O. Rogers, "Beam: A Monte Carlo code to simulate radiotherapy treatment units," *Med. Phys.* **22**(5), 503–524 (1995).
- ²⁹J. Yoon, J. Kim, J. Jung, and I. Yeo, "Exit EPID image prediction below heterogeneous phantoms using Monte Carlo codes," *Med. Phys.* **40**(6), 240 (2013).
- ³⁰M. Fippel, F. Haryanto, O. Dohm, F. Nüsslin, and S. Kriesen, "A virtual photon energy fluence model for Monte Carlo dose calculation," *Med. Phys.* **30**(3), 301–311 (2003).